Precise measurement of $^{226}Ra/^{230}Th$ disequilibria in deep-sea sediments by high-sensitivity ICP-MS

Liuting Yuan[a, b], Pinghe Cai[a, b*], Xingyu Jiang[a, b], Walter Geibert[c], Yilin Cheng[a, b], Yaojin Chen[a]

[a] State Key Laboratory of Marine Environmental Science, Xiamen University, Xiamen 361005, P. R. China

[b] College of Ocean and Earth Sciences, Xiamen University, Xiamen 361005, P. R. China

[c]Alfred-Wegener Institute, Helmholtz Centre for Polar and Marine Research, Bremerhaven 27570, Germany

*Corresponding author:

Pinghe Cai

State Key Laboratory of Marine Environmental Science, Xiamen University

Xiamen 361005, P. R. China

E-mail: Caiph@xmu.edu.cn;

Phone: 86-592-2880179

Fax: 86-592-2180655

Chemical Geology

Abstract

We describe a new method suitable for the precise and accurate determination of ^{226}Ra in porewater and sediment samples using a single-collector sector field ICP-MS (ThermoFisher Element XR) equipped with an Apex-Q desolvation device and a high-sensitivity Jet-X interface. In combination with ^{230}Th measurements in parallel sediment samples, this method allows precise and accurate quantification of the $^{226}Ra/^{230}Th$ disequilibria in surface sediment cores, thereby enabling the use of this isotope pair as a tracer of solute transfer across the sediment-water interface in the deep ocean. The method integrates a step of isotope dilution with ^{228}Ra as an internal spike, a pre-concentration of Ra and Ba by MnO_2 precipitation, and an efficient separation of Ra from other undesirable elements using a cation exchange resin and a Triskem Sr-spec resin. With the inclusion of one or two additional cation resin columns and the use of up to 16 bed-volumes of a lower molarity (1.7 M) HCl eluent, our procedure eliminates the complicated matrix effects persistently encountered in previous studies, and provides a highly purified solution suitable for ^{226}Ra measurement using an Element XR ICP-MS apparatus. Consequently, we are able to determine the activity of ^{226}Ra in ~20-50 ml of porewater or 100 mg of sediment with an internal precision of ~1.0% and an accuracy of ~99.2%. The precise measurements of porewater and solid phase ^{226}Ra in a sediment core from the North Pacific Ocean allowed the distribution coefficient (K_d) of ^{226}Ra to be constrained tightly within a range of 4700-11600 ml g^{-1}. Moreover, with the aid of a one-dimensional exchange model, the combination of the ^{226}Ra and ^{230}Th measurements allowed us to estimate a ^{226}Ra flux of 1140±20 dpm m^{-2} y^{-1} from the sediment core.

1. Introduction

Marine sediments can be either major sinks or major sources of chemical substances in coastal seas and the open ocean. Understanding what controls the exchange of chemicals and nutrients between the sediment and overlying water reservoirs is a key aspect of marine geochemical studies (Broecker and Peng, 1982). Naturally occurring radionuclides in the uranium and thorium decay chains are powerful tools for the investigation of mass transfer processes taking place at the sediment-water boundary (Krishnaswamy et al., 1971; Koide et al., 1973; Aller and Cochran, 1976; Tamborski et al., 2022). In particular, the advent of the $^{224}Ra/^{228}Th$ isotope pair in the past decade has provided a new way to study solute exchange across the sediment-water interface in the coastal ocean (Cai et al., 2012; 2014). Application of the so-called $^{224}Ra/^{228}Th$ disequilibrium approach has significantly expanded since its first introduction in 2012 and has greatly improved our knowledge of the mechanisms that control solute transfer between the sediment and water reservoirs in highly dynamic coastal systems (e.g., Hong et al., 2017; 2018; Shi et al., 2018; 2019; Cai et al., 2020; Tamborski et al., 2021; Wei et al., 2022). However, a major limitation of the $^{224}Ra/^{228}Th$ disequilibrium approach lies in the short half-life of ^{224}Ra ($t_{1/2}$=3.66 d), which is translated into a relatively rapid production and decay rate of this isotope in nature. Consequently, any deviation of ^{224}Ra from ^{228}Th is not expected to be detectable in deep-sea sediments, where physical disturbances are rather weak (Shi et al., 2019). In such an environment, the $^{226}Ra/^{230}Th$ isotope pair in the uranium decay chain should be an excellent substitute: the long half-life of ^{226}Ra ($t_{1/2}$=1600 a) can amplify very subtle and weak disturbances in the quiescent ocean floor to a large $^{226}Ra/^{230}Th$ disequilibrium signal in the sediment. Goldberg and Koide (1963) reported the first

measurements of ^{226}Ra and ^{230}Th for sediment cores collected from the Indian Ocean. Since then, investigators have reported marked deficits and excesses of ^{226}Ra relative to ^{230}Th in the upper layer of deep-sea sediment cores (Cochran and Krishnaswamy, 1980; Cochran, 1980). Nevertheless, application of the ^{226}Ra/^{230}Th isotope pair to date is surprisingly sparse and has generally been limited to tracing bioturbation processes near the sediment-water boundary (Kadko et al., 1987).

We believe that this dilemma is caused by the technical challenges for precise measurement of ^{226}Ra/^{230}Th disequilibria in sediments. To use the ^{226}Ra/^{230}Th isotope pair as a tracer of interfacial solute exchange in the deep-sea floor, it is necessary to determine the activity of ^{226}Ra in the aqueous phase (porewater) along with the measurements of ^{226}Ra and ^{230}Th in the bulk sediment (Cochran and Krishnaswamy, 1980). While the determination of ^{230}Th in the bulk sediment to date has become routine (e.g., Geibert et al., 2019), the task of precise measurement of ^{226}Ra in porewaters and sediments still lies at the edge of the capacity of traditional radioactive counting techniques and modern mass spectrometric methods (e.g., Lariviere et al., 2006; Charette et al., 2012). For a comprehensive overview of all the techniques for measuring ^{226}Ra and their pros and cons, please refer to Vieira et al. (2021). In any type of determination, instrumental sensitivity and the sample matrix are of particular concern. Radium-226 is present in sediment porewater at the sub-femtogram (fg or 10^{-15}g) level, typically ranging from 0.2 to 6.5 fg g^{-1} in the deep Pacific Ocean (Cochran and Krishnaswamy, 1980; Kadko et al., 1987). To facilitate an accurate and precise measurement of ^{226}Ra, collection of a minimum of ~500-1000 ml of porewater is generally required when using traditional radioactive counting techniques (for instance, the Rn emanation method). In practice,

sampling such a large amount of porewater is tedious and not always possible, especially onboard an ocean-research vessel (Kadko et al., 1987). Modern high-sensitivity mass spectrometers, such as thermal ionization mass spectrometers (TIMS) or inductively coupled plasma mass spectrometers (ICP-MS), have significantly increased instrumental sensitivity to a detection limit of <0.1 fg g^{-1} for ^{226}Ra (Cohen and O'nions, 1991; Chabaux et al., 1994; Staubwasser et al., 2004). This important technical advance has allowed several research teams to successfully measure ^{226}Ra activities in seawater samples less than 250 ml (e.g., Foster et al., 2004; Bourqin et al., 2011; Hsieh et al., 2011).

However, when the sample matrix is porewater or sediment, researchers have met additional challenges. Spectral interferences were persistently encountered at m/z of 226 in ICP-MS. A variety of polyatomic ions, such as $^{88}Sr^{138}Ba^{+}$, $^{87}Sr^{139}La^{+}$, $^{86}Sr^{140}Ce^{+}$, $^{186}W^{40}Ar^{+}$, $^{186}W^{40}Ca^{+}$, $^{199}Hg^{27}Al^{+}$, $^{202}Hg^{24}Mg^{+}$, $^{208}Pb^{18}O^{+}$, $^{209}Bi^{17}O^{+}$, and $^{203}Tl^{23}Na^{+}$, have been identified as contributing to the apparent signal of ^{226}Ra (Larivière et al., 2005; Zhang et al., 2015; Yaala et al., 2019). Theoretically, these polyatomic interferences can be resolved using a medium/high resolution mode of measurement (Vieira et al., 2021), or be eliminated by use of a collision cell (Epov et al., 2003; Yaala et al., 2019). Unfortunately, neither strategy can be accomplished without losing substantial sensitivity, which in turn would require a larger sample size if a high precision of ^{226}Ra measurement were to be maintained. On the other hand, sediment and porewater samples are typically characterized by high levels of Mg, Ca, Sr, and Ba, and trace levels of these elements in the final solution to be measured are sufficient to cause a marked reduction in the ionization and transmission efficiencies of Ra (Cohen and O'nions, 1991; Copia et al., 2015). This phenomenon is ascribed to a space charge effect, which again

leads to a substantial loss in sensitivity (Thomas, 2001). Furthermore, the presence of Mg, Ca, and Ba in the final solution may readily cause salt accumulation on the sampler and skimmer cones (Foster et al., 2004). This problem can become more and more severe with the progress of measurement, and may greatly deteriorate the stability of ICP-MS signals.

To solve the abovementioned problems, we present here a new procedure for the rapid and precise determination of ^{226}Ra in porewater and sediment samples using a single-collector sector field ICP-MS (ThermoFisher Element XR) equipped with an Apex-Q desolvation device and a high-sensitivity Jet-X interface. Our procedure integrates 1) isotope dilution with ^{228}Ra as an internal spike (Cohen and O'nions, 1991), 2) pre-concentration of Ra and Ba by MnO_2 precipitation (Ghaleb et al., 2004), and 3) efficient separation of Ra from other unwanted elements using a cation exchange resin and a Triskem Sr-spec resin (Chabaux et al., 1994; Zhang et al., 2015). With the inclusion of one or two additional cation resin columns and the use of up to 16 times bed-volume of a lower molarity (1.7 M) HCl eluent, this procedure results in a highly purified solution suitable for ^{226}Ra measurement in an Element XR ICP-MS instrument. Consequently, we can determine the activity of ^{226}Ra in ~20-50 ml porewater and 100 mg sediment samples with an internal precision of ~1.0%. In combination with ^{230}Th measurements in parallel sediment samples, this method enables the use of the $^{226}Ra/^{230}Th$ isotope pair as a tool to study solute transfer across the sediment-water interface of the deep-ocean floor.

2. Analytical methods

2.1. Chemical procedures

2.1.1. Separation and purification of Ra from the porewater matrix

All beakers and vials used in this study were soaked for two 12-h periods in high-purity 2M HNO_3, and thoroughly washed with 18 MΩ deionized water. Trace metal grade acids (HNO_3, HCl, $HClO_4$ and HF) and analytical grade $KMnO_4$, $MnCl_2 \cdot 4H_2O$ and NH_4OH were used. All reagents were prepared in 18 MΩ deionized water, and were found to be free of Ra.

A known quantity (20-50 ml) of porewater was acidified to pH<2 with concentrated HCl. After gravimetric addition of ~50 fg ^{228}Ra spike (1 dpm ^{228}Ra =1.653 fg ^{228}Ra) to guarantee that any contribution of ^{228}Ra from the sample is negligible, the sample was shaken vigorously and allowed to equilibrate for 12 hours. The sample then was diluted to ~80 ml with deionized water. The pH was brought up to 8.5-9 with concentrated NH_4OH. Radium was isolated by sorbing it to a MnO_2 precipitate that was formed by the sequential addition of 1.0 ml of $KMnO_4$ (15 g $KMnO_4$ l^{-1}) solution and 1.0 ml of $MnCl_2$ (40 g $MnCl_2 \cdot 4H_2O$ l^{-1}) solution. The sample was shaken vigorously between each addition and heated at a hot plate for ~30 minutes. After it cooled down to room temperature, the MnO_2 precipitate containing sorbed Ra was recovered by centrifugation, washed twice with deionized water, and dissolved in 2.0 ml concentrated HCl and 1 ml 30% H_2O_2. The solution was transferred to a Teflon beaker, evaporated to dryness, and re-dissolved into 6 ml of 8 M HNO_3. Subsequently, Ra was isolated using a modification of the ion exchange method used to isolate Ra from seawater and carbonate matrixes (Chabaux et al., 1994; Zhang et al., 2015; Vieira et al., 2021). Details of the modified procedure are given in Table 1. First, an anion exchange column with 8 ml of chloride form resin (Bio-Rad AG 1-X8, 100-200 mesh) was used to remove any ^{228}Th that might be present in the sample and in the ^{228}Ra spike solution. This step serves to avoid isobaric interference at m/z=228. The second

158 and third cation exchange columns (Bio-Rad AG 50-X8, 100-200 mesh) separated Ra and Ba
159 from other major elements that would interfere with ICP-MS measurement, especially Mg, Ca,
160 and Sr. The final 500-µl column of Sr-spec resin separated Ra from Ba. In a lower molarity
161 HCl eluent, radium tends to have a superior selectivity on the cation exchange column.
162 Previous studies have further demonstrated that the use of up to 20 times bed-volume of 1.7 M
163 HCl eluent does not cause significant loss of radium from the cation exchange column (Zhang
164 et al., 2015). Thus, we used 10-16 times the bed-volume of 1.7 M HCl (Table 1) to rinse a 100-
165 200 mesh resin column, instead of using the 4-8 times bed-volume of 3-6 M HCl to rinse a
166 200-400 mesh resin column that was used in most previous studies (Staubwasser et al., 2004;
167 Foster et al., 2004; Vieira et al., 2021). This modification proved to be critical for the efficient
168 purification of Ra from complicated matrixes, especially porewater or sediments. The final
169 eluent was evaporated, and taken up in 2 ml of 2% nitric acid for analysis.
170 2.1.2. Separation and purification of Ra and Th from the sediment matrix
171 For the determination of ^{226}Ra in sediments, ~100 mg of dried sediment was weighed and
172 spiked with a known quantity of ^{228}Ra (~165 fg or 100 dpm of ^{228}Ra). The sample was digested
173 sequentially using 10 ml of concentrated HNO_3, 2 ml of 30% HF, and 2 ml of $HClO_4$ until the
174 solution became clear. The digestion mixture was evaporated to dryness, and 10 ml of 1.4 N
175 HNO_3 was added. This mixture was centrifuged, and any solid residual was discarded. The
176 resulting solution was collected, evaporated to dryness, and re-dissolved in 6 ml of 8 M HNO_3.
177 The subsequent separation and purification of Ra is broadly similar to the procedure described
178 for porewater samples above (see Table 1), but differs in two aspects. First, the step for co-
179 precipitation of Ra and Ba onto a MnO_2 suspension was pursued after the cation-exchange

chemistry of "Column 2" in Table 1. It is impractical to perform this same step with sediment samples before the anion-exchange chemistry of "Column 1" because adjusting the pH to 8-9 at this stage will precipitate a large quantity of undesirable material from the sample solution, e.g., $Fe(OH)_3$ and $Al(OH)_3$. Second, the step for the cation-exchange chemistry of "Column 3" (see Table 1) was executed twice in order to thoroughly remove all unwanted elements from the very complex sediment matrix. Finally, the eluent was evaporated, and taken up in 2 ml of 2% nitric acid for analysis.

For the determination of ^{230}Th in sediments, a separate sample of ~100 mg freeze-dried sediment was weighed and spiked with 5.0 dpm (or 10.6 pg) of ^{229}Th. We do not recommend that the same sample as ^{226}Ra be used because the ^{228}Ra spike itself may contain a significant amount of ^{230}Th. The procedure for sediment digestion is similar to that described above for ^{226}Ra samples. After centrifugation, the digested material was transferred into a 50-ml Teflon beaker, evaporated to dryness, and re-dissolved in 6 ml of 8 M HNO_3. The subsequent separation and purification of ^{230}Th followed classic anion-exchange column chemistry (e.g., Anderson and Fleer, 1982) and is detailed in Table 1. The final sample solution was prepared in 2 ml of 2% nitric acid for measurement by ICP-MS.

2.2. Spike calibration

The ^{228}Ra spike was prepared by re-milking a $Th(NO_3)_4$ salt at an interval of ~6-12 months after the first separation of Ra from Th in an anion-exchange column (Cohen and O'nions, 1991). Because ^{226}Ra grows at a rate much lower than that of ^{228}Ra, this strategy creates a spike with a high $^{228}Ra/^{226}Ra$ ratio. The chromatographic method for separation and purification of the Ra fraction from the $Th(NO_3)_4$ salt has been described in Vieira et al. (2021), and is similar

to the anion-exchange column chemistry detailed in Table 1. The ^{228}Ra spike was calibrated against a ^{226}Ra standard provided by China Institute of Atomic Energy via isotope dilution using an Element XR mass spectrometer. A succession of 0.000, 0.2000, 0.4000, 0.6000, and 0.8000 g of ^{226}Ra standards with an activity of 1.117 dpm g^{-1} were added to five ^{228}Ra spike replicates. As shown in Figure 1, the activity of ^{228}Ra in the spike was determined to be 204.2±1.1 dpm g^{-1} (337.5±1.8 fg g^{-1}), and the ^{228}Ra/^{226}Ra atomic ratio was 5.46±0.14 (reference date: October 27, 2021).

2.3. Mass spectrometry

Measurement of ^{226}Ra and ^{230}Th was performed using a ThermoFisher Element XR sector field inductively coupled plasma mass spectrometer (SF-ICP-MS) at Xiamen University. This instrument facilitates spectrometric measurements in three different mass resolution modes of R=300 (low-resolution), 4000 (medium-resolution), and 10000 (high-resolution). In order to achieve an optimum sensitivity for the Element XR ICP-MS, we coupled an Apex-Q desolvation device to the sample introduction system. An additional benefit from the Apex-Q desolvation device is that it minimizes molecular interference. In the interface region, the common Standard-H configuration was replaced with a Jet-type sampler cone and an X-type skimmer cone. In this manner, we pushed the sensitivity of the instrument to around 40-50 cps fg^{-1} ml^{-1} for Ra in the low-resolution mode, which is ~20 times the sensitivity provided by the same instrument without the inclusion of the Apex-Q desolvation device and Jet-X cones.

Before each set of measurements, the Element XR mass spectrometer was tuned to maximum sensitivity and stability using a solution of lithium (Li), indium (In), and uranium (U). The RF generator power was 1250W. Argon flow rates used for coolant, auxiliary, and

sample were 16, 0.8, and 1.0 L min^{-1}, respectively. In the low-resolution mode, the mass regions for ^{226}Ra and ^{228}Ra were 225.7466 to 226.3033 and 227.7499 to 228.3122, respectively. From each set of ^{226}Ra samples, we randomly selected 6-8 samples to perform the first measurements, and used the "full peak scan" method in both the low-resolution (R=300) and the medium-resolution (R=4000) modes to examine peak shape and check any interferences that might bias the $^{226}Ra/^{228}Ra$ ratio (Vieira et al., 2021). After ensuring that no interferences were present in each mass spectrum, we continued to execute the second and the third measurements for each sample using a method of "peak hopping" at the low-resolution mode to acquire a $^{226}Ra/^{228}Ra$ ratio. While the third measurement is not mandatory, the combination of the second and third measurements, i.e., two replicate measurements of the same sample, provides a better internal precision than that offered by a single measurement. For ^{230}Th samples, a single measurement was performed in the medium-resolution mode to obtain a $^{230}Th/^{229}Th$ ratio. Instrumental mass bias was monitored at m/z=235 and 238 using a natural U standard solution of 5 ppt with a hypothetical $^{235}U/^{238}U$ ratio of 0.007253. The difference between the measured ratio and the hypothetical ratio gave a mass bias of ~0.7% per amu, which was extrapolated to correct the $^{226}Ra/^{228}Ra$ and $^{230}Th/^{229}Th$ ratios using a simple linear mass bias law.

3. Results

3.1. Blank and recovery

The blank for the entire Ra procedure was determined for each set of sample measurements. Ra-free blanks were prepared using ~80 ml of deionized water without the addition of a ^{228}Ra spike, and processed in the same manner as porewater samples. Blank signals at m/z=226 and

228 were typically lower than 10 and 5 counts per second (cps), respectively (Figure S1). These values represented <1% of the ^{226}Ra and ^{228}Ra signals for porewater and sediment samples, and final data reported here are blank-corrected. For ^{230}Th measurements in sediment, blank signals at m/z=229 and 230 were negligible compared to sample signals. The tailing of ^{232}Th on ^{230}Th and ^{229}Th peaks was monitored in the medium-resolution mode by measuring mass signals at m/z=229.8 and 230.2, and at m/z=228.8 and 229.2, respectively. The contribution from ^{232}Th tailing to the ^{230}Th and ^{229}Th signals in the sediment sample was <0.1% and <0.5%, respectively.

The total recovery of Ra was assessed by independent analyses of replicate sediment samples with the addition of a known quantity of the short-lived ^{224}Ra isotope. To this end, a set of eight replicate sediment samples each with a dried mass of ~100 mg were spiked with 40.0 dpm of ^{232}U. The ^{232}U standard had been stored for >20 years, and therefore ^{232}U-^{228}Th-^{224}Ra was assumed to be in transient equilibrium. The sediment standards were processed following the chemical procedure described above. Radium-224 in the final solution and in each column eluent fraction was co-precipitated with MnO_2 by addition of an appropriate quantity of $KMnO_4$ and $MnCl_2$ solutions. After the MnO_2 suspension was filtered onto a 142-mm 0.7-μm pore size GFF filter, the sample was measured using a delayed coincidence counting system (the RaDeCC system) as per Cai et al. (2012). In the RaDeCC system, a sealed sample is placed in a closed He-circulation loop, where the alpha decay products of adsorbed ^{224}Ra (to ^{220}Rn) and ^{223}Ra (to ^{219}Rn) are swept into a ZnS phosphor scintillation detector (*i.e.,* Lucas cell). Alpha decay of the radon daughters within the Lucas cell generates light, which is subsequently transformed into an electronic pulse from a photomultiplier tube and then sent to a delayed coincidence circuit, where ^{220}Rn and ^{219}Rn daughters are discriminated and counted

(Moore and Arnold, 1996). The total recovery of Ra for the entire procedure was assessed through a comparison of ^{224}Ra activity determined in the final solution with the sum of all the eluent fractions, and was found to vary between 92.3% and 97.8% (Figure S2), similar to that reported using earlier methods by Foster et al. (2004), Bourquin et al. (2011), and Vieira et al. (2021).

3.2. Spectral and non-spectral interferences

Several research teams have suggested that the presence of $^{88}Sr^{138}Ba^{+}$ at m/z=225.8 could be the major contributor to polyatomic interferences, and may lead to a characteristic "step" slightly before the actual peak of ^{226}Ra (e.g., Epov et al., 2003; Foster et al., 2004; Copia et al., 2015). However, mass spectra of sediment and porewater samples measured here exhibited symmetrical peak shapes at m/z=226 and 228 in the low-resolution mode (Figure 2). No "steps" were seen at m/z=225.8 and 227.8 as observed in some previous studies. The mass spectra measured in the medium-resolution mode confirmed the absence of polyatomic interferences in the mass windows of 225.7466-226.3033 and 227.7499-228.3122 (Figure 3). Thus, it is clear that undesirable elements that might interfere with spectrometric measurement of ^{226}Ra had been completely removed from the very complex sediment and porewater matrixes. Under such circumstances, the use of the low-resolution mode offers optimum instrumental sensitivity. This is particularly important for ^{226}Ra measurements in porewater because high instrumental sensitivity means that a smaller sample size is required.

Our procedure is also very effective for the elimination of non-spectral interferences. We have measured more than one hundred sediment and porewater samples in the Element XR ICP-MS, and no salt accumulation was seen on the sample and skimmer cones. The intensity

290 of mass spectrometric signals was fairly constant during the measurement. In addition, we did
291 not see any difference in the intensity of ^{228}Ra signal between sediment/porewater samples and
292 highly purified ^{226}Ra standards that were spiked with the same quantity of ^{228}Ra. This indicates
293 that any residual impurities in the sample solution that might have jeopardized ionization and
294 transmission of Ra in the ICP-MS instrument had been completely removed. For a sediment
295 sample spiked with ~165 fg ^{228}Ra, we normally obtained a spectral signal of ~6500-8000 cps
296 $^{228}Ra^{+}$ in 1 ml of 2% HNO_3 solution. This signal translates into an instrumental sensitivity of
297 40-50 cps fg^{-1} ml^{-1} for Ra, which is ~3 times higher than that reported by Vieira et al. (2021).
298 Finally, we must emphasize that the inclusion of pre-concentration of Ra and Ba by MnO_2
299 precipitation and a second (for porewater samples) or a third (for sediment samples) cation
300 resin column in our protocol is necessary for complete removal of spectral and non-spectral
301 interferences from the sample matrixes. This is best manifested in the quality of the mass
302 spectra of Ra without the execution of these steps, which is greatly deteriorated in terms of
303 both signal intensity and peak shape (Figure S3). Relative to alkaline earth elements (like Ca,
304 Sr, Ba, and Ra), Mn^{2+} has a much lower affinity for the cation resin column in the HCl eluent
305 (e.g., Vieira et al. 2021). Although the precipitation step introduces a significant amount of
306 Mn^{2+} into the sample, the subsequent two cation resin columns acts to remove it very efficiently
307 so that any remaining Mn^{2+} in the final solution would be too low to interfere with the
308 measurement of Ra on ICP-MS.
309 3.3. Reproducibility and accuracy
310 Eight sets of two replicate sediment samples from the same core collected from the South
311 China Sea were measured for ^{226}Ra following the above-described procedure. The results are

312 presented in Table S1. The mean ratio of ^{226}Ra activities for the replicate samples was
313 1.002±0.019 (1SD). This represents an external reproducibility of 2% at 68% confidence level
314 that includes both chemical separation and spectrometric measurement.

315 The accuracy of sediment ^{226}Ra and ^{230}Th measurements using the method described here
316 was assessed through the determination of ^{226}Ra and ^{230}Th activities in an in-house mica
317 standard in which ^{238}U-^{234}U-^{230}Th-^{226}Ra are known to be in secular equilibrium. Two sets of
318 six replicate mica standards were analyzed following the procedure for sediment samples
319 detailed in Table 1. We measured an activity of 2.031±0.029 dpm g^{-1} for ^{226}Ra, and 2.048±0.026
320 dpm g^{-1} for ^{230}Th (Table S1). Within the uncertainty of our measurements, the ratio of
321 ^{226}Ra/^{230}Th (0.992±0.019, 1SD) is consistent with the secular equilibrium ratio of unity.

322 The accuracy of porewater ^{226}Ra measurements is difficult to assess because there is no
323 porewater standard available for such an exercise. As a substitute, seven ~250-gram samples
324 of near-bottom seawater collected at different sites in the North Pacific Ocean were analyzed
325 following the procedure described for porewater samples. The measured ^{226}Ra activities ranged
326 from 0.321±0.001 to 0.333±0.001 dpm kg^{-1} (Table S2), in excellent agreement with previous
327 results (0.32-0.34 dpm kg^{-1}) based on the traditional ^{222}Rn emanation method (Cochran, 1980).
328 Although the sample size for the ^{226}Ra analysis was similar to that used in previous ICP-MS
329 methods, our seawater measurements provided a much better precision than that reported by
330 other investigators (~1.0% vs. 2.5%-6.6%; see Vieira et al., 2021). Consequently, our data
331 exhibited a clear trend of increasing ^{226}Ra activity with water depth despite the variation being
332 less than 4% (plot not shown).
333

4. Discussion

4.1. Field application

We performed ^{226}Ra and ^{230}Th measurements in deep-sea sediments in order to assess the applicability of our method. During a cruise to the North Pacific Ocean from September 15 to November 25 in 2021, sediment cores were collected at site A8 (16° 29.27' N, 137° 57.48' E; 4927 m) using a box corer (50 cm length×50 cm width×80 cm height). The overlying seawater was siphoned off, and ferromanganese nodules were carefully removed from the sediment surface. Subsequently, sediment sub-cores were obtained by gently inserting PVC tubes with a diameter of 65 mm into the box core. Porewater was extracted at discrete depths from several parallel sediment sub-cores using Rhizon samplers (Seeberg-Elverfeldt et al., 2005). A separate sub-core was collected for the analyses of sediment ^{226}Ra and ^{230}Th. Sediment and porewater samples were stored at 4 °C before they were returned our land-based laboratory for analyses.

Figure 4 gives the results of ^{226}Ra and ^{230}Th measurements from this deep-sea sediment core. Sediment ^{226}Ra activities ranged from 33.01±0.32 dpm g^{-1} to 83.73±0.07 dpm g^{-1} (dried mass) and exhibited a maximum at ~15 cm (Table S3). In comparison, ^{230}Th activities were relatively uniform in the upper ~5 cm sediment layer. This phenomenon can best be explained by biological mixing which often homogenizes this zone. Below the bioturbation zone, ^{230}Th activities decreased gradually with depth, from 124.8±0.4 dpm g^{-1} at ~ 5 cm to 32.87±0.50 dpm g^{-1} at ~ 48 cm. Porewater ^{226}Ra activities increased from 4.31±0.01 dpm kg^{-1} near the sediment-water interface to a maximum of 7.85±0.02 dpm kg^{-1} at ~ 10 cm, and then decreased steadily to a value of 4.57±0.06 dpm kg^{-1} at ~45 cm (Figure 4, lower panel). The most prominent feature displayed by the solid phase measurements was a remarkable deficiency of ^{226}Ra relative to

356 ^{230}Th in the upper ~15 cm (Figure 4, upper panel), indicating active migration of ^{226}Ra from
357 near-surface sediment into the overlying water column. Between 15 and 20 cm, there was a
358 layer of ^{226}Ra excess with respect to ^{230}Th, followed by another layer of ^{226}Ra deficiency at ~
359 25 cm. Below this depth horizon, ^{226}Ra and ^{230}Th approached secular equilibrium.

360 In an early study, Cochran and Krishnaswami (1980) used traditional radiometric
361 techniques (^{222}Rn emanation and alpha spectrometric methods) to determine ^{226}Ra and ^{230}Th in
362 deep-sea sediments from the North Equatorial Pacific. Similar to our observations, a large
363 deficiency of ^{226}Ra relative to ^{230}Th in the solid phase was evident from the sediment surface
364 to ~30 cm in all of the three depth profiles obtained by these investigators. The ^{226}Ra/^{230}Th
365 activity ratios at the top of the cores were ~0.3, indistinguishable from our value of 0.319±0.003
366 (Table S3). Albeit with less precision (~10%), their ^{226}Ra determinations based on 500-1000
367 ml porewater samples (0.49±0.06-14.2±2.4 dpm kg^{-1}) bracketed our results, and showed a
368 depth pattern similar to that displayed in Figure 4. The consistency between our measurements
369 suggests that analyzing ^{226}Ra and ^{230}Th by high-sensitivity ICP-MS is very reliable.

370 4.2. Radium distribution coefficient

371 One important piece of information extractable from the measurements of porewater and
372 solid phase ^{226}Ra is the radium distribution coefficient (K_d) in the sediment core, which is a
373 key index for assessing the remobilization of this nuclide. The radium distribution coefficient
374 is defined as

375 $$K_d = \frac{C_S}{C_p} \qquad (1)$$

376 where C_s is the adsorbed ^{226}Ra activity in the solid phase (unit: dpm g^{-1}), and C_p denotes the
377 dissolved ^{226}Ra activity in the aqueous phase (unit: dpm ml^{-1}). Note that C_s represents only the

exchangeable fraction of the total ^{226}Ra measured in the solid phase. K_d defined in this fashion takes into account the sediment mass/porewater volume ratio of the system. The concept of K_d requires an adsorption-desorption equilibrium of ^{226}Ra between the solid and aqueous phase (Geibert and Usbeck, 2004). In deep-sea sediments, this premise can generally be satisfied because the adsorption and desorption of ^{226}Ra in oxic porewater take place over a time scale of minutes or less (e.g., Krishnaswami et al., 1982), much shorter than the porewater residence time in the bio-turbation zone (Cochran and Krishnaswami, 1980). Although C_s is not directly measurable, an upper limit can be set by assuming that all ^{226}Ra in the sediment was potentially exchangeable. On the other hand, a value of 0.319±0.003 for the $^{226}Ra/^{230}Th$ activity ratio measured at the top of the sediment core indicates that at least 68.1% of the total ^{226}Ra produced from decay of the ^{230}Th in the solid phase was potentially exchangeable. Indeed, early investigators utilized the recoil of ^{222}Rn as an analogue for ^{226}Ra recoil to quantify the emanation/desorption of ^{226}Ra from deep-sea sediment grains, and found that 61 to 75 percent of the total ^{226}Ra in the solid phase was potentially desorbable (Cochran and Krishnaswami, 1980). Thus, we used the value of 68.1% to place a lower limit on C_s.

The upper and lower limits of K_d estimated in this manner ranged from 6800 to 11600 ml g^{-1}, and from 4700 to 7900 ml g^{-1} respectively (Table S3). The K_d values of ^{226}Ra went through a maximum at 15 to 20 cm depth, in concert with the ^{226}Ra excess with respect to ^{230}Th in the solid phase. This depth pattern might be a result of changes in porewater pH, sediment mineralogy, and sediment grain size. For instance, early investigators recognized that remobilization of manganese taking place during the diagenetic oxidation of organic matter can cause steep absorption gradients within the sediment (Kadko et al., 1987). Consequently,

400 ^{226}Ra profiles measured in sediment cores from the eastern Equatorial Pacific can be simulated
401 by adjusting the distribution coefficient of ^{226}Ra as a function of depth-varying manganese
402 content. There are few historical studies on the adsorption behavior of radium with which to
403 compare our K_d values. Cochran and Krishnaswami (1980) used the traditional ^{222}Rn
404 emanation method to determine porewater and solid phase ^{226}Ra activities in sediment cores
405 from the North Equatorial Pacific. In combination with an emanation/desorption experiment,
406 they gave a range of 4300-17400 ml g^{-1}, and 5400-22600 ml g^{-1} for the lower and upper limits
407 of K_d value, respectively. Their low end is comparable to the lowest value of our estimates
408 (4300 vs. 4700 ml g^{-1}). However, their high end is two times the highest value of our estimates
409 (22600 vs. 11600 ml g^{-1}). Because high K_d values are the result of a stark contrast in ^{226}Ra
410 activity between the solid phase and the aqueous phase, and because the uncertainty of ^{226}Ra
411 measurements increases at low activities, large errors can accompany those high K_d values
412 determined using the traditional ^{222}Rn emanation method. In this aspect, the precise
413 measurements of ^{226}Ra facilitated by high-sensitivity ICP-MS in the present study allow the K_d
414 value of ^{226}Ra to be more tightly constrained than ever before.

415 4.3. Flux of ^{226}Ra from the sediment column

416 Another important piece of information extractable from the precise measurements of
417 ^{226}Ra and ^{230}Th is the flux of ^{226}Ra from the sediment column, which can help to constrain the
418 rate of ocean circulation (Cochran, 1980). While several models can be employed for this
419 purpose, the most straightforward scheme may be a one-dimensional (1-D) exchange model
420 similar to that used to estimate ^{224}Ra fluxes from coastal sediments (Cai et al., 2015):

421 $$F_{Ra} = \int_0^{z_m} \lambda_{Ra} (Th - Ra_T) dz - \omega(Th^0 - Ra_{Th}^0) \quad (2)$$

where z_m is the sampling depth, λ_{Ra} is the decay constant of ^{226}Ra, ω is the sedimentation rate (unit: cm ky^{-1}), Ra_T and Th are the total ^{226}Ra and ^{230}Th activities in a unit of dpm cm^{-3} wet sediment respectively, and the superscript 0 represents activity in the surface sediment; F_{Ra} is the flux of ^{226}Ra from the sediment column and represents the sum of all processes operating near the sediment-water interface that can induce a flux of ^{226}Ra into the overlying water column. To calculate the flux of ^{226}Ra from Eq. (2), the sedimentation rate (ω) must be known.

In analogy to ^{210}Pb dating for coastal sediments, the excess of ^{230}Th ($^{230}Th_{ex}$) in deep-sea sediments can be used to determine a sedimentation rate (e.g., Goldberg and Koide, 1962; Geibert et al., 2019). Three different models are commonly employed for this purpose: 1) the constant flux: constant sedimentation rate model; 2) the constant initial concentration model; and 3) the constant rate of supply model (for a review, see Sanchez-Cabeza and Ruiz-Fernández, 2012). All models require an assessment of the $^{230}Th_{ex}$ activity in the sediment column. Total ^{230}Th in deep-sea sediments is contributed from three sources. The first source is the flux of new ^{230}Th atoms produced by decay of ^{234}U from the overlying water column to the sediment column. This component exceeds ^{230}Th in equilibrium with ^{234}U in the sediment and is called excess ^{230}Th. The remnant ^{230}Th, i.e., supported ^{230}Th, can in turn have two sources. It consists of a lithogenic fraction and an authigenic fraction, the latter of which is produced by decay of authigenic ^{234}U that accumulates in anoxic sediments as uranium in the bottom seawater penetrates into the sediment. The relative importance of these components varies considerably in different sedimentary settings. In general, the authigenic component is negligible under the typical oxic conditions (Geibert et al., 2019). In the absence of authigenic uranium, the supported ^{230}Th activity can be approximated as the activity of ^{234}U or ^{238}U in the sediment by

assuming that ^{230}Th, ^{234}U, and ^{238}U in the lithogenic fraction of deep-sea sediments are in secular equilibrium. We herein used a value of 1.4 dpm g^{-1} determined for the activity of ^{238}U in a sediment core from the North Equatorial Pacific to correct the contribution of supported ^{230}Th (Cochran and Krishnaswami, 1980). As the supported ^{230}Th represents only a small fraction of the total ^{230}Th in the sediment under study (see Table S3), any error caused by this correction must be minor.

We chose the constant flux: constant sedimentation rate model to estimate the sedimentation rate in the study site. This model is based on cumulative mass depth (g cm^{-2}), rather than absolute depth, in order to take into consideration any sediment compaction and downcore variation in dry bulk density. By assuming a constant flux of ^{230}Th and a constant mass accumulation rate, the model is expressed as:

$$Th_{ex}^{i} = Th_{ex}^{0} \times e^{-\lambda_{Th}\frac{m}{k}} \quad (3)$$

where Th_{ex}^{i} is excess ^{230}Th activity at depth i and Th_{ex}^{0} is the excess ^{230}Th activity at the surface (unit: dpm g^{-1}), λ_{Th} is the decay constant of ^{230}Th (0.00916 ky^{-1}), m is the cumulative dry mass, and k is the mass accumulation rate (unit: g cm^{-2} ky^{-1}). Plotting cumulative mass [X] versus ln (Th_{ex}) [Y] and dividing the best-fit slope by λ_{Th} gave a value of 0.13 g cm^{-2} ky^{-1} for k (Figure 5). Based on the porosity data (Table S3), the mass accumulation rate was converted into a sedimentation rate of 0.32 cm ky^{-1} using the relation $k=\omega\cdot\rho\cdot(1-\phi)$ where ρ is the density of dry sediment (2.65 g cm^{-3}) and ϕ is the sediment porosity. Finally, we substituted the sedimentation rate into Eq. (2) and derived a value of 1140±20 dpm m^{-2} y^{-1} for F_{Ra}. The sedimentation term corrected for a relatively small flux of -110 dpm m^{-2} y^{-1}. In comparison, direct integration of the deviations of total ^{226}Ra with respect to ^{230}Th from the sediment-water

interface to the sampling depth yielded a flux of 1250±20 dpm m^{-2} y^{-1} for the first term in the right-hand side of Eq. (2).

The flux of ^{226}Ra from a sediment core may also be deduced by modelling the depth profile of dissolved ^{226}Ra in porewater. To this end, Cochran and Krishnaswami (1980) developed a sophisticated diagenetic model that takes into consideration mixing of sediment particles by bioturbation, molecular diffusion in the dissolved phase, adsorption onto particle surfaces, as well as radioactive production and decay. Fluxes of ^{226}Ra were calculated from the model-generated porewater ^{226}Ra gradients at the sediment-water interface using Fick's first law, ranging from 800 to 2200 dpm m^{-2} y^{-1} in the North Equatorial Pacific. Although this flux range brackets our value, Cochran and Krishnaswami's diagenetic model relied on many variables that were generally difficult to constrain. To find "good fits" to their porewater profiles of ^{226}Ra, a wide range of sediment mixing coefficient, molecular diffusion coefficient, fraction of Th decays that recoil Ra atoms, and Ra distribution coefficient had to be assigned. In comparison, Eq. (2) depends on only the solid phase ^{226}Ra and ^{230}Th data and an estimate of the sedimentation rate, which in turn can be deduced from the solid phase ^{230}Th data. Thus, our approach is a relatively simple and easy way to quantify the flux of ^{226}Ra from the sediment column.

5. Concluding remarks

The $^{226}Ra/^{230}Th$ isotope pair in deep-sea sediments can be regarded as a counterpart to the $^{224}Ra/^{228}Th$ isotope pair that has been extensively used to study solute exchange across the sediment-water interface in coastal seas. However, traditional radiometric techniques used for

488 the determination of ^{226}Ra have relied on porewater samples of >500-1000 ml. Consequently,
489 it may take as long as ~2 weeks to sample an eight-point profile of ^{226}Ra (e.g., Cochran and
490 Krishnaswami 1980). This technical challenge has prevented the ^{226}Ra/^{230}Th isotope pair from
491 developing into an approach for studying solute exchange across the sediment-water interface
492 of the deep-sea floor. In this study, we have described a new method for measurement of ^{226}Ra
493 in porewater and sediment samples by high-sensitivity ICP-MS. Because our procedures used
494 only 20-50 ml of porewater and 100 mg of dried sediment, the time required for sampling a
495 depth profile of ^{226}Ra was greatly shortened, to ~2 hours under typical conditions. More
496 importantly, our method provided a much better precision for both porewater and sediment
497 measurements than that reported by early investigators using the conventional radiometric
498 methods (~1.0% vs. ~10% for porewater measurements, and ~1.0% vs. ~3.0% for sediment
499 measurements). We have also determined ^{230}Th activities in deep-sea sediments using the same
500 high-sensitivity ICP-MS instrument. This combination led to an accurate and precise
501 quantification of both the ^{226}Ra distribution coefficient and the ^{226}Ra deficiency in the upper
502 sediment core from the North Pacific Ocean. Consequently, our method will enable researchers
503 to use the ^{226}Ra/^{230}Th isotope pair, in a fashion similar to the ^{224}Ra/^{228}Th disequilibrium
504 approach for coastal sediments, to examine a wide spectrum of interfacial exchange processes
505 in the deep-ocean floor, like $CaCO_3$ dissolution and formation, chemical weathering of silicate
506 minerals…etc.
507
508 **Acknowledgements**
509 This work was supported by the Natural Science Foundation of China (NSFC) through

Grant No. 92058205, and by the Fundamental Research Funds for the Central Universities of China through Grant No. 20720200070. Samples were collected onboard R/V "Dongfanghong 3" implementing the open research cruise NORC 2021-582 supported by NSFC Ship-time Sharing Project (grant No. 42049582). Pingping Mi is acknowledged for her logistic support of this research. We are grateful to Cindy Lee for her help with English and constructive comments on an early version of this manuscript. Thanks are also due to François Chabaux and an anonymous reviewer for providing comments that improved the manuscript.

References

Aller, R. C., Cochran, J. K., 1976. $^{234}Th/^{238}U$ disequilibrium in near-shore sediment: particle reworking and diagenetic time scales. Earth Planet. Sci. Lett. 29, 37-50. https://doi.org/10.1016/0012-821X(76)90024-8

Anderson, R.F., Fleer, A.P., 1982. Determination of Natural Actinides and Plutonium in Marine Particulate Material. Anal. Chem., 54(7): 1142-1147. https://doi.org/10.1021/ac00244a030

Bourquin, M., van Beek, P., Reyss, J. L., Riotte, J., Freydier, R., 2011. Determination of ^{226}Ra concentrations in seawater and suspended particles (NW Pacific) using MC-ICP-MS. Mar. Chem. 126, 132–138. https://doi.org/10.1016/j.marchem.2011.05.001

Broecker, W. S., Peng, T.-H., 1982. Tracers in the sea. Lamont-Doherty Geol. Observation, Eldigo Press, Palisades, NY, p.113-127.

Cai, P., Shi, X., Moore, W.S., Dai, M., 2012. Measurement of $^{224}Ra:^{228}Th$ disequilibriumin coastal sediments using a delayed coincidence counter. Mar. Chem. 138–139, 1–6. https://doi.org/10.1016/j.marchem.2012.05.004

Cai, P., Shi, X., Moore, W.S., Peng, S., Wang, G., Dai, M., 2014. $^{224}Ra:^{228}Th$ disequilibrium in coastal sediments: Implications for solute transfer across the sediment-water interface. Geochim. Cosmochim. Acta 125, 68–84. https://doi.org/10.1016/j.gca.2013.09.029

Cai, P., Shi, X., Hong, Q., Li, Q., Liu, L., Guo, X., Dai, M., 2015. Using $^{224}Ra/^{228}Th$

disequilibrium to quantify benthic fluxes of dissolved inorganic carbon and nutrients into the Pearl River Estuary. Geochim. Cosmochim. Acta 170, 188–203. https://doi.org/10.1016/j.gca.2015.08.015.

Cai, P., Wei, L., Geibert, W., Koehler, D., Ye, Y., Liu, W., Shi, X., 2020. Carbon and nutrient export from intertidal sand systems elucidated by $^{224}Ra/^{228}Th$ disequilibria. Geochim. Cosmochim. Acta. https://doi.org/10.1016/J.GCA.2020.02.007.

Charette, M.A. et al., 2012. GEOTRACES radium isotopes inter-laboratory comparison experiment. Limnol. Oceanogr.: Methods, 10: 451-463. https://doi.org/10.4319/lom.2012.10.451

Chabaux, F., Othman, D. B., Birck, J. L., 1994. A new Ra-Ba chromatographic separation and its application to Ra mass-spectrometric measurement in volcanic rocks. Chem. Geol. 114, 191-197.

Cochran, J. K., 1980. The flux of ^{226}Ra from deep-sea sediments. Earth Planet. Sci. Lett. 49, 381-392. https://doi.org/10.1016/0012-821X(80)90080-1

Cochran, J. K., Krishnaswami, S., 1980. Radium, thorium, uranium, and ^{210}Pb in deep-sea sediments and sediment pore waters from the north equatorial Pacific. Am. J. Sci. 280, 849-889. https://doi.org/10.2475/ajs.280.9.849

Cohen, A. S., O'Nions, R. K., 1991. Precise Determination of Femtogram Quantities of Radium by Thermal Ionization Mass-Spectrometry. Anal. Chem., 63(23): 2705–2708. https://doi.org/10.1021/ac00023a008

Copia, L., Nisi, S., Plastino, W., Ciarletti, M., Povinec, P. P., 2015. Low-level ^{226}Ra determination in groundwater by SFICP-MS: Optimization of separation and pre-concentration methods. J. Anal. Sci. Technol. 6, 1–7. https://doi.org/10.1186/s40543-015-0062-5

Epov, V. N., Lariviere, D., Evans, R. D., Li, C., Cornett, R. J., 2003. Direct determination of ^{226}Ra in environmental matrices using collision cell inductively coupled plasma mass-spectrometry. J. Radioanal. Nucl. Chem. 256, 53–60. https://doi.org/10.1023/A:1023343824444

Foster, D. A., Staubwasser, M., Henderson, G. M., 2004. ^{226}Ra and Ba concentrations in the Ross Sea measured with multicollector ICP mass spectrometry. Mar. Chem. 87, 59–71.

https://doi.org/10.1016/j.marchem.2004.02.003

Geibert, W., Usbeck, R., 2004. Absorption of thorium and protactinium onto different particle types: Experimental findings. Geochim. Cosmochim. Acta 68, 1489-1501. https://doi.org/10.1016/j.gca.2003.10.011

Geibert, W., Stimac, I., Rutgers van der Loeff, M. M., Kuhn, G., 2019. Dating deep-sea sediments with ^{230}Th excess using a constant rate of supply model. Paleoceanogr. Paleoclimat. 34, 1895-1912. https://doi.org/10.1029/2019PA003663

Ghaleb, B., Pons-branchu, E., Deschamps, P., 2004. Improved method for radium extraction from environmental samples and its analysis by thermal ionization mass spectrometry. J. Anal. At. Spectrom., 19(7): 906–910. https://doi.org/10.1039/B402237H

Goldberg, E. D., Koide, M., 1962. Geochronological studies of deep sea sediments by the ionium/thorium method. Geochim. Cosmochim. Acta 26, 417–450. https://doi.org/10.1016/0016-7037(62)90112-6

Goldberg, E. D., Koide, M., 1963. Rates of sediment accumulation in the Indian Ocean, in Geiss J. and Goldberg E. D., eds., Earth Science and Meteoritics, New Jork, John Wiley & Sons, p. 90-120.

Hong, Q., Cai, P., Shi, X., Li, Q., Wang, G., 2017. Solute transport into the Jiulong River estuary via pore water exchange and submarine groundwater discharge: New insights from ^{224}Ra/^{228}Th disequilibrium. Geochim. Cosmochim. Acta 198, 338-359. https://doi.org/10.1016/j.gca.2016.11.002

Hong, Q., Cai, P., Geibert, W., Cao, Z., Stimac, I., Liu, L., Li, Q., 2018. Benthic fluxes of metals into the Pearl River Estuary based on ^{224}Ra/^{228}Th disequilibrium: From alkaline earth (Ba) to redox sensitive elements (U, Mn, Fe). Geochim. Cosmochim. Acta 237, 223-239. https://doi.org/10.1016/j.gca.2018.06.036

Hsieh, Y. T., Henderson, G. M., 2011. Precise measurement of ^{228}Ra/^{226}Ra ratios and Ra concentrations in seawater samples by multi-collector ICP mass spectrometry. J. Anal. At. Spectrom. 26, 1338–1346. https://doi.org/10.1039/C1JA10013K

Kadko, D., Cochran, J. K., Lyle, M., 1987. The effect of bioturbation and adsorption gradients on solid and dissolved radium profiles in sediments from the eastern equatorial Pacific.

Geochim. Cosmochim. Acta, 51(6): 1613-1623. https://doi.org/10.1016/0016-7037(87)90342-5

Koide, M., Bruland, K. W., Goldberg, E. D., 1973. Th-228/Th-232 and Pb-210 geochronologies in marine and lake sediments. Geochim. Cosmochim. Acta 37, 1171–1187. https://doi.org/10.1016/0016-7037(73)90054-9

Krishnaswamy, S., Lal, D., Martin, J.M., Meybeck, M., 1971. Geochronology of lake sediments. Earth Planet. Sci. Lett. 11, 407–414. https://doi.org/10.1016/0012-821X(71)90202-0

Krishnaswami, S., Graustein, W. C., Turekian, K. K., Dowd, J. F., 1982. Radium, thorium and radioactive lead isotopes in groundwaters: Application to the in situ determination of adsorption-desorption rate constants and retardation factors. Water Resour. Res. 18, 1663-1675. https://doi.org/10.1029/WR018i006p01663

Larivière, D., Epov, V. N., Reiber, K. M., Cornett, R. J., Evans, R. D., 2005. Micro-extraction procedures for the determination of Ra-226 in well waters by SF-ICP-MS. Anal. Chim. Acta, 528(2): 175–182. https://doi.org/10.1016/j.aca.2004.09.076

Lariviere, D., Taylor, V. F., Evans, R. D., Cornett, R. J., 2006. Radionuclide determination in environmental samples by inductively coupled plasma mass spectrometry. Spectrochim. Acta B At. Spectrosc. 61, 877–904. https://doi.org/10.1016/j.sab.2006.07.004

Moore, W. S., Arnold, R., 1996. Measurement of ^{223}Ra and ^{224}Ra in coastal waters using a delayed coincidence counter. J. Geophys. Res. 101, 1321–1329. https://doi.org/10.1029/95JC03139

Sanchez-Cabeza, J. A., Ruiz-Fernández, A. C., 2012. ^{210}Pb sediment radiochronology: An integrated formulation and classification of dating models. Geochim. Cosmochim. Acta 82, 183–200. https://doi.org/10.1016/j.gca.2010.12.024

Seeberg-Elverfeldt, J., Schluter, M., Feseker, T., Kolling, M., 2005. Rhizon sampling of porewaters near the sediment-water interface of aquatic systems. Limnol. Oceanogr.: Methods, 3: 361-371. https://doi.org/10.4319/lom.2005.3.361

Shi, X., Mason, R. P., Charette, M. A., Mazrui, N. M., Cai, P., 2018. Mercury flux from salt marsh sediments: Insights from a comparison between ^{224}Ra/^{228}Th disequilibrium and core incubation methods. Geochim. Cosmochim. Acta 222, 569–583.

https://doi.org/10.1016/j.gca.2017.10.033

Shi, X., Wei, L., Hong, Q., Liu, L., Wang, Y., Shi, X., Ye, Y., Cai, P., 2019. Large benthic fluxes of dissolved iron in China coastal seas revealed by $^{224}Ra/^{228}Th$ disequilibria. Geochim. Cosmochim. Acta 260, 49-61. https://doi.org/10.1016/j.gca.2019.06.026

Staubwasser, M., Henderson, G. M., Berkman, P. A., Hall, B. L., 2004. Ba, Ra, Th, and U in marine mollusc shells and the potential of $^{226}Ra/Ba$ dating of Holocene marine carbonate shells. Geochim. Cosmochim. Acta 68, 89–100. https://doi.org/10.1016/S0016-7037(03)00279-5

Tamborski, J. J., Eagle, M., Kurylyk, B. L., Kroeger, K. D., Wang, Z. A., Henderson, P., Charette, M. A., 2021. Pore water exchange-driven inorganic carbon export from intertidal salt marshes. Limnol. Oceanogr. 66, 1774–1792. https://doi.org/10.1002/lno.11721

Tamborski, J. J., Cai, P., Eagle, M., Henderson, P., Charette, M. A., 2022. Revisiting ^{228}Th as a tool for determining sedimentation and mass accumulation rates. Chem. Geol. 607, 121006. https://doi.org/10.1016/j.chemgeo.2022.121006

Thomas, R., 2001. A beginner's guide to ICP-MS. Spectroscopy 16, 26-34.

Vieira, L. H., Geibert, W., Stimac, I., Koehler, D., Rutgers van der Loeff, M. M., 2021. The analysis of ^{226}Ra in 1-litre seawater by isotope dilution via single-collector sector-field ICP-MS. Limnol. Oceanogr.: Methods 19, 356-367. https://doi.org/10.1002/lom3.10428

Wei, L., Cai, P., Shi, X., Cai, W. J., Liu, W., Hong, Q., Wu, T., Bai, Y., Cheng, P., Sun, Z., 2022. Winter mixing accelerates decompostion of sedimentary organic carbon in seasonally hypoxic coastal seas. Geochim. Cosmochim. Acta 317, 457-471. https://doi.org/10.1016/j.gca.2021.11.003

Yaala, H. B., Fniter, R., Foucher, D., Clarisse, O., 2019. Direct analysis of ^{226}Ra in sediment by ICP-MS: an analytical challenge? J. Anal. At. Spectrom. 34, 1597–1605. https://doi.org/10.1039/C9JA00156E

Zhang, T., Bain, D., Hammack, R., Vidic, R. D., 2015. Analysis of Radium-226 in high salinity wastewater from unconventional gas extraction by Inductively Coupled Plasma-Mass Spectrometry. Environ. Sci. Technol., 49(5): 2969−2976. https://doi.org/10.1021/es504656q

Table 1. Chemical separation of Ra (Column 1-4) from a porewater (or sediment) matrix, and separation of Th (Column 1*-2*) from a sediment matrix.

	Column 1	Column 2	Column 3	Column 4	Column 1*	Column 2*
Resin type	BioRad® AG 1-X8, 100-200 mesh	BioRad® AG50W-X8, 100-200 mesh	BioRad® AG50W-X8, 100-200 mesh	Sr Spec® 100-150 μm	BioRad® AG 1-X8, 100-200 mesh	BioRad® AG 1-X8, 100-200 mesh
Column type	10 ml BioRad Econo-Column	10 ml BioRad Econo-Column	(3 ml) 6 cm length, 8 mm diameter	(1 ml) 8 cm length, 4 mm diameter	10 ml BioRad Econo-Column	(3ml) 6 cm length, 8 mm diameter
Resin volume	8 ml	8 ml	2.5 ml	0.5 ml	8 ml	2.5 ml
Conditioning	24 ml 8N HNO_3	24 ml 1.7N HCl	7.5 ml 1.7N HCl	6 ml 3N HNO_3	24 ml 8N HNO_3	7.5 ml 8N HNO_3
Sample loaded in:	6 ml 8N HNO_3	3 ml 0.5N HCl	1.5 ml 0.5N HCl	1.5 ml 3N HNO_3	6 ml 8N HNO_3	1.5 ml 8N HNO_3
Wash:	–	80 ml 1.7N HCl	40 ml 1.7N HCl	–	24 ml 8N HNO_3	12.5 ml 8N HNO_3
Elute	24 ml 8N HNO_3	40 ml 3N HNO_3	15 ml 3N HNO_3	1 ml 3N HNO_3	24 ml 6N HCl	7.5 ml 6N HCl
Eluted elements	Ra + other cations	Ra + Ba	Ra + some Ba	Ra	Th	Th

Figure captions

Figure 1. Standard addition curve for calibration of the ^{228}Ra spike. Error bars are shown if larger than the symbol size. The reciprocals of the slope and the y-axis intercept denote the ^{228}Ra concentration (unit: fmol g^{-1}) and the ^{228}Ra/^{226}Ra atomic ratio in the spike, respectively. For ^{226}Ra to ^{228}Ra, an atomic ratio of 1:1 corresponds to an activity ratio of 1:278.6.

Figure 2. Mass spectrometric measurements of ^{226}Ra and ^{228}Ra in porewater using the low-resolution mode (R=300).

Figure 3. Mass spectrometric measurements of ^{226}Ra and ^{228}Ra in sediment using the medium-resolution mode (R=4000). The mass spectra of ^{226}Ra and ^{228}Ra are expanded in the lower panel.

Figure 4. Depth profiles of ^{226}Ra and ^{230}Th in dry sediment (upper panel), and ^{226}Ra in porewater (lower panel) from a core in the North Pacific Ocean. With a bottom depth of 4927 m, the sampling site was located at 16° 29.27' N, 137° 57.48' E.

Figure 5. Excess ^{230}Th activity versus cumulative mass depth in the sediment core from the North Pacific Ocean.

Figure 1

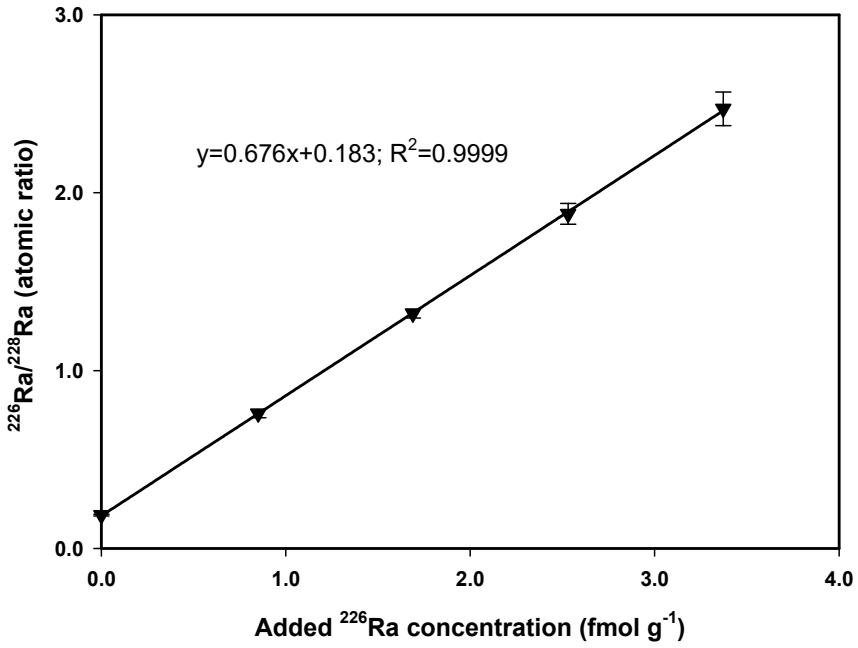
y=0.676x+0.183; R2=0.9999
226Ra/228Ra (atomic ratio)
Added 226Ra concentration (fmol g-1)
0.0
1.0
2.0
3.0
4.0

Figure 2

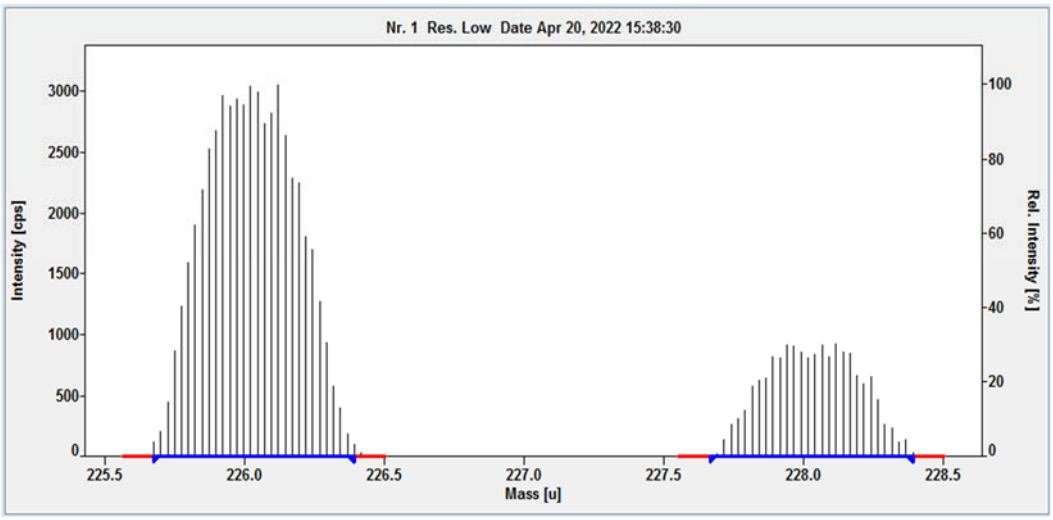
Nr. 1 Res. Low Date Apr 20, 2022 15:38:30
Intensity [cps]
Rel. Intensity [%]
Mass [u]
3000
2500
2000
1500
1000
500
0
100
80
60
40
20
0
225.5
226.0
226.5
227.0
227.5
228.0
228.5

Figure 3

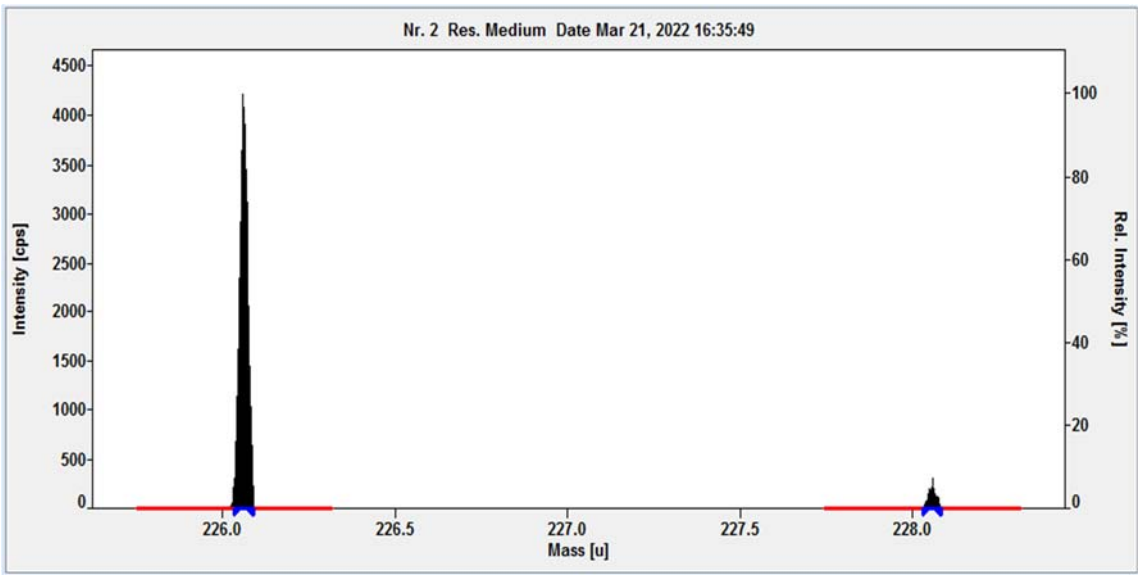
Nr. 2 Res. Medium Date Mar 21, 2022 16:35:49
Intensity [cps]
Rel. Intensity [%]
Mass [u]
4500
4000
3500
3000
2500
2000
1500
1000
500
0
100
80
60
40
20
0
226.0
226.5
227.0
227.5
228.0

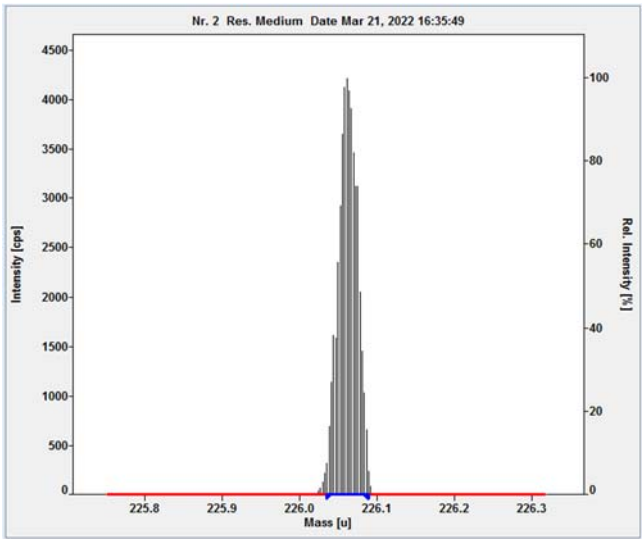
Nr. 2 Res. Medium Date Mar 21, 2022 16:35:49
Intensity [cps]
Rel. Intensity [%]
Mass [u]
4500
4000
3500
3000
2500
2000
1500
1000
500
0
100
80
60
40
20
0
225.8
225.9
226.0
226.1
226.2
226.3

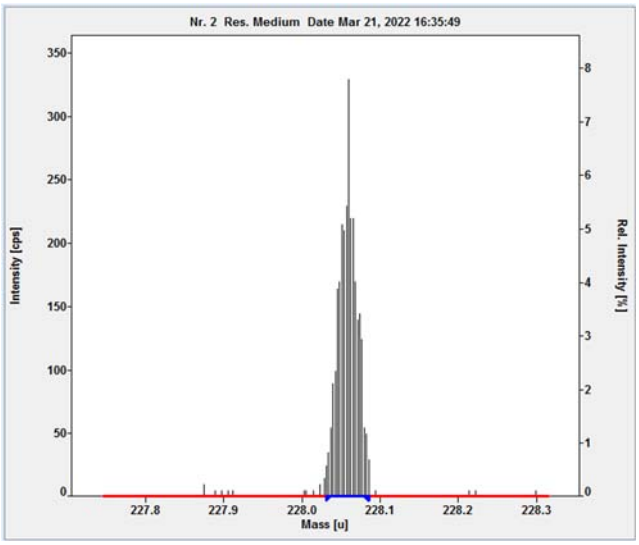
Nr. 2 Res. Medium Date Mar 21, 2022 16:35:49
Intensity [cps]
Rel. Intensity [%]
Mass [u]
350
300
250
200
150
100
50
0
8
7
6
5
4
3
2
1
0
227.8
227.9
228.0
228.1
228.2
228.3

Figure 4

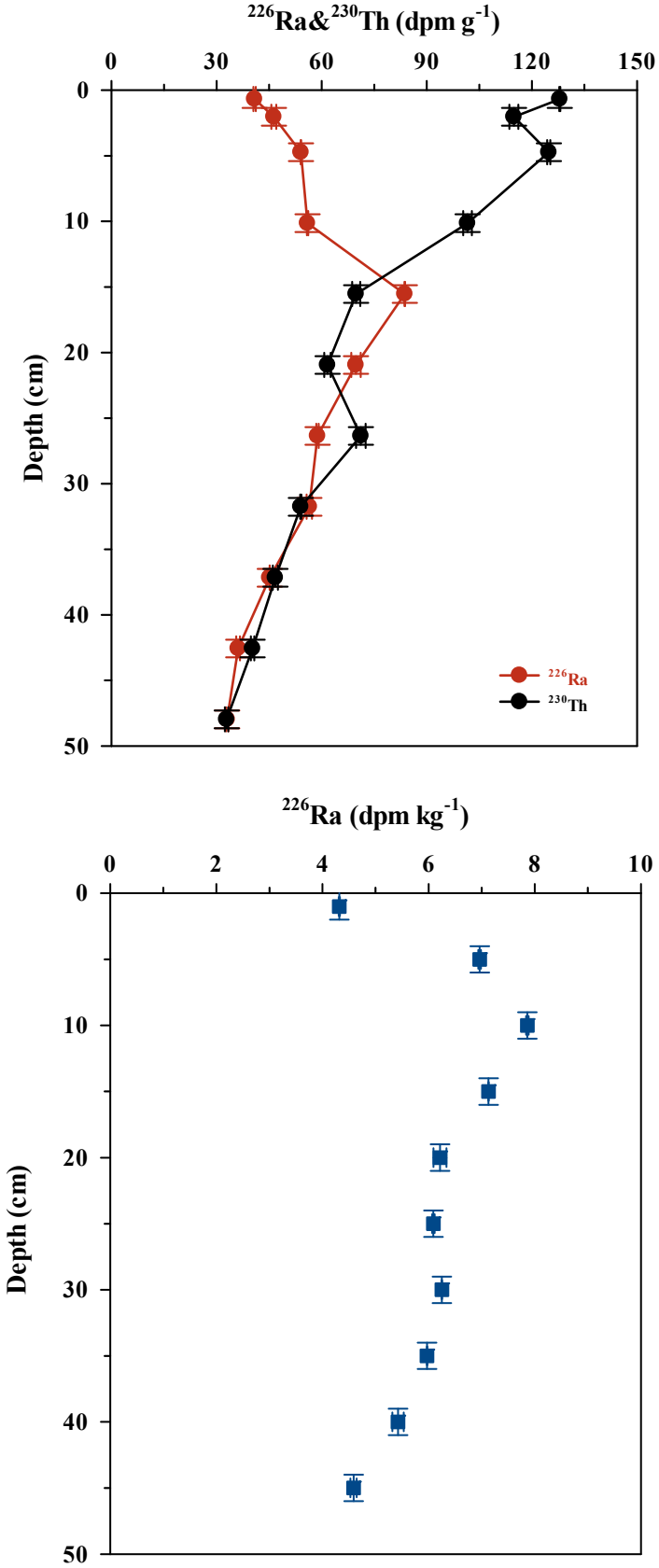
^{226}Ra&^{230}Th (dpm g^{-1})
0
30
60
90
120
150
Depth (cm)
0
10
20
30
40
50
^{226}Ra
^{230}Th
^{226}Ra (dpm kg^{-1})
0
2
4
6
8
10
Depth (cm)
0
10
20
30
40
50

Figure 5

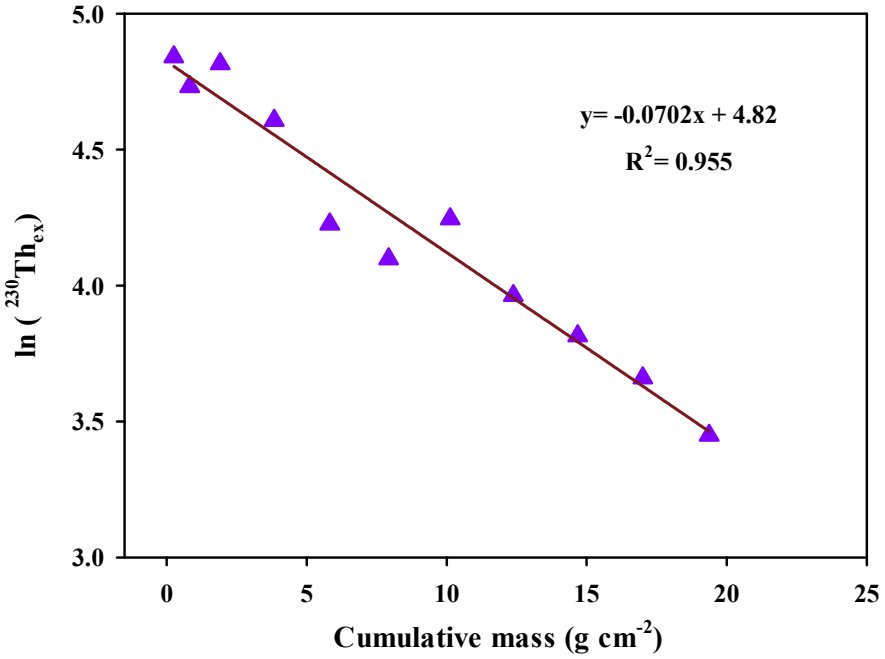
y= -0.0702x + 4.82
R2= 0.955
ln (230Thex)
Cumulative mass (g cm-2)
5.0
4.5
4.0
3.5
3.0
0
5
10
15
20
25